Shape Optimisation for Friction Dampers with Stress Constraint

E. Denimal[a], R. Chevalier[a], L. Renson[b], L. Salles[c]
a. Univ. Gustave Eiffel, Inria, COSYS/SII, I4S, Campus Beaulieu, Rennes, France – enora.denimal@inria.fr
b. Dynamics group, Imperial College London, United Kingdom
c. Skolkovo Institute of Science and Technology, Moscow, Russia

ABSTRACT
Friction dampers are classically used in turbomachinery for bladed disks to control the levels of vibrations at resonance and limit the risk of fatigue failure. It consists of small metal components located under the platforms of the blades, which dissipates the vibratory energy through friction when a relative displacement between the blades and the damper appears. It is well known that the shape of such component has a strong influence on the damping properties and should be designed with a particular attention. With the arrival of additive manufacturing, new dedicated shapes for these dampers can be considered, determined with specific numerical methods as topological optimisation (TO). However, the presence of the contact nonlinearity challenges the use of traditional TO methods to minimise the vibration levels at resonance. In this work, the topology of the damper is parametrized with the Moving Morphable Components (MMC) framework, and optimised based on meta-modelling techniques: here kriging coupled with the Efficient Global Optimisation (EGO) algorithm. The level of vibration at resonance are computed based on the harmonic balanced method augmented with a constraint to aim directly for the resonant solution. It corresponds to the objective function to be minimised. Additionally, a mechanical constraint based on static stress analysis is also considered to propose reliable damper designs. Results demonstrate the efficiency of the method and show that dampers geometries that meet the engineers' requirements can be identified.

Keywords: nonlinear vibrations, topological optimisation, kriging, friction damping, resonance mitigation.

INTRODUCTION

The design of aircraft turbines is of major importance in the aeronautic industry, as they are subjected to numerous loadings: thermal, vibrational, stress etc. More particularly, a vibration analysis must be carried out to limit the phenomenon of high cycle fatigue that could lead to dramatic accidents. Due to the high modal density of turbines, all resonances cannot be avoided and so the level of vibrations at resonance must be controlled. One solution consists of the introduction of damping in the system. For such applications, dry friction damping is now a classical solution. It can be introduced in different locations of the bladed disc, namely at the tip of the blades, under the platforms of the blades etc. For high pressure turbine, a classical solution is the introduction of underplatform dampers [1]. It consists of small metal pieces, introduced under the platforms of adjacent blades, that are maintained in position due to the centrifugal loading during operation. When the blades vibrate, a relative displacement appears between the latter and the damper. It generates friction and so energy is dissipated. Due to this dissipation, vibrations are damped. This friction contact is the origin of a nonlinearity in the system dynamics. It is established that the shape of the contact surface has a strong impact on the damping efficiency [2]. With the coming of additive manufacturing, the question of the interest of topological optimisation (TO) for friction damper is natural.

TO for continuum structures consists in determining the optimal distribution of the material over a given domain and for given boundary conditions [3]. The topology of a component is defined by the location of the limit between the interior and the exterior, and the location of inner holes. These limits and these inner holes are optimised to minimise an objective function with respect to constraints. The first family of classical approaches to solve TO problems are the density-based methods. An initial mesh of the system is constructed and the material density of each mesh element are then optimised. The updating process in the optimisation is based on the sensitivity of the objective function to the density variation in each element. A second family of methods exists where the geometry is described implicitly with a Level-Set Function (LSF) and then propagated by solving the Hamilton-Jacobi equation using the shape sensitivities of the LSF. Both methods require the sensitivities of the objective function to the element densities or to the shape, if not known analytically, they might be too expensive to compute numerically. A recent approach, called Moving Morphable Components, proposes to parametrise the LSF with a few parameters [4], making possible to use more

standard optimisation methods, and more particularly global optimisation algorithms that are well adapted for expensive objective function and/or when the gradients are difficult to determine [5,6,7]. This method has already proven to be efficient to deal with the optimisation of friction dampers for nonlinear vibrations [6,7]. Previous works were only focused in the minimisation of the vibration amplitude at resonance. However, numerous geometries presented very thin parts and so were not reliable. The interest of considering a static stress constraint in the optimisation to avoid such geometries is investigated in the present work.

First, the system under study is briefly presented. Second, the moving morphable components framework is presented, as well as the optimisation process. The computation of the nonlinear response with the Harmonic Balance formulation augmented with a phase constraint is introduced, as well as the computation of the static stress constraint. Finally, results are analysed and the choice of the static stress constraint discussed.

SYSTEM UNDER STUDY

The mechanical system under study is a 2D system that simulates the dynamic behaviour of two blades of a high-pressure turbine [8]. It is composed of two blades represented by two beams with platforms and represented in Fig. 1. The blades are connected to a basis that represents the disc. The damper is located between the two blades, under the platforms. In real-world conditions, the damper is maintained in position due to the centrifugal loading. Close to resonance, when the blades vibrate, a relative displacement exists between the damper and the platforms and so friction appears. It dissipates energy and so the vibrations are damped.

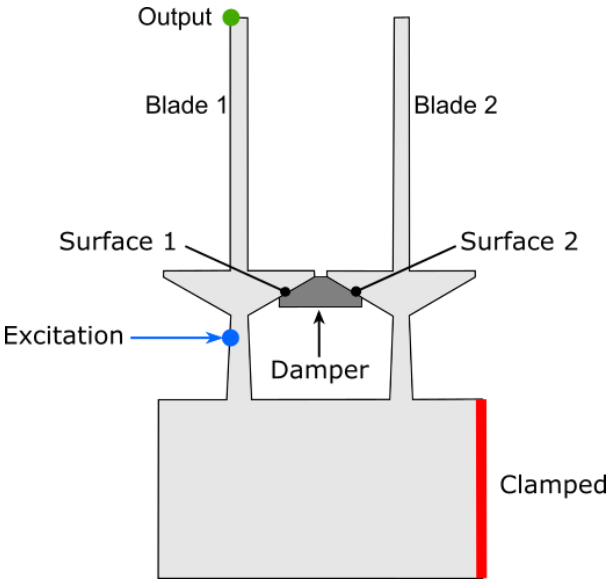

(a)

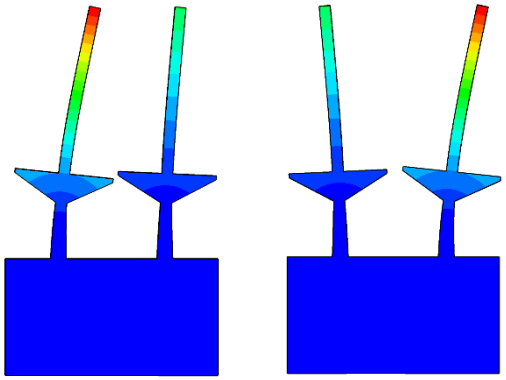

(b) (c)

Fig.1: System under study (a) – In Phase (b) and Out-of-phase (c) bending mode of the blades

In this study, the blades are excited at the base of blade 1 (see arrow in Fig. 1) with an amplitude of 8N, and output displacements are observed at the top of blade 1 (green point in Fig. 1). A finite element model (FEM) for the blades is constructed in Abaqus, it is composed of 3324 8-nodes bi-quadratic plane strain elements. The structure is made of steel with a Young modulus of 197GPa and a density of 7800kg/m^3. First bending modes of the blades can be in-phase (IP) or out-of-phase (OOP) and takes place at 246.73Hz and 247.51Hz, respectively. They are obtained without the damper and modeshapes are represented in Fig.1. An initial FEM for the damper is constructed, and is composed of 3604 elements with the same material than the blades. The meshes are constructed to ensure the matching at contact points. The damper mesh will be updated during the optimisation process, as explained later on.

Contact surfaces are discretised and a node-to-node contact modelling approach is adopted [7]. For each contact element, the 2D contact model is composed of one Jenkins element and one normal spring to ensure normal load variations. Each element is characterised by four parameters: the friction coefficient μ, the normal contact stiffness k_n, the tangential contact stiffness k_t and the initial normal pre-load N_0. Three contact states are possible, namely separation, stuck condition, slip condition. For the rest of the study, the friction coefficient is taken equal to $\mu = 0.5$, and it is assumed that the contact stiffnesses are equal in the normal and tangential directions and depend on N_0. The hypothesis is made that the initial contact pressure is homogeneous and depends directly on the centrifugal loading C_f and the number of contact point n_{c_0}. As an illustration, for a full damper, 51 contact points are present on each contact line, the normal pre-load is $N_0 = 9.8987$N and $k_n = k_t = 20000\ N/m$.

DAMPER PARAMETRISATION AND OPTIMISATION PROCESS

Geometry parametrisation

The damper geometry is described implicitly with a Level Set Function (LSF) Ψ, defined on the design space D [3]. For a point of coordinates (x, y), Ψ takes positive values if the point is in the material domain Ω, negative values if it is in the void domain and is equal to 0 on the boundary. The MMC framework proposes to decompose this global LSF in the assembly of n_{MMC} several local LSF $\Psi_i, i = 1, \dots, n_{MMC}$, defined explicitly based on a few parameters [4]. Each local LSF defines a material domain Ω_i and the final material domain is $\Omega = \bigcup_i \Omega_i$. More concretely, each local LSF Ψ_i is defined as:

$$\Psi_i(x,y) = -\left[\left(\frac{\cos\theta_i\,(x - x_{0,i}) + \sin\theta_i\,(y - y_{0,i})}{\frac{L_i}{2}}\right)^m + \left(\frac{-\sin\theta_i\,(x - x_{0,i}) + \cos\theta_i\,(y - y_{0,i})}{\frac{t_i}{2}}\right)^m - 1\right]$$

Where (x, y) are the coordinates of a point, θ_i is the inclination of the ith component, L_i its length, t_i its thickness and $(x_{0,i}, y_{0,i})$ the position of its centre. m is an even number, equal to 6 here. The different parameters are illustrated in Fig.2a for a component, and in Fig.2b its LSF is represented (negative values have been set to 0 for the sake of readability). By assembling different components, expanding them, shrinking them, moving them, one can describe complex geometries. This approach has two advantages: the topology is parametrised and the number of parameters is low. This makes possible the use of more traditional optimisation approaches as gradient-free ones.

The connectivity of the different local LSF is checked, and unconnected geometries are removed during the initialisation, or penalised in the optimisation. The global LSF is then mapped on the damper mesh, which will be explained latter.

Efficient Global Optimisation algorithm

The optimisation consists in the minimisation of the displacements at resonance at the blade tip, considering a constraint on the static stress distribution in the damper. The optimisation process is detailed in this section, details for the computation of the objective and constraint functions are given afterwards. Considering the non-convexity of the considered problem and the numerical difficulty to compute the gradients of the functions, a gradient-free optimisation approach is adopted, based on the EGO algorithm that exploits kriging meta-models of the objective and constraint functions coupled with an updating process [5,6,7,8].

An initial set of N_{init} input points $\mathbf{P} = [\mathbf{p}^{(1)}, \dots, \mathbf{p}^{(N_{init})}]$ is generated, it corresponds to different damper geometries. For each of them, the objective function and the constraint function are evaluated: the vibration amplitude at resonance (denoted u_{peak}) and the maximum of stress (denoted σ_{max}) are computed. Based on these sets of inputs and outputs, two kriging meta-models are created: one for the objective function and another for the constraint function. Considering a given criterion, these kriging meta-models are exploited to find the new point to be added in the learning set. The objective function and the constraint are evaluated for this new geometry and the learning set is extended with this new point. The iterative process is stopped after a maximum number of iterations chosen by the user.

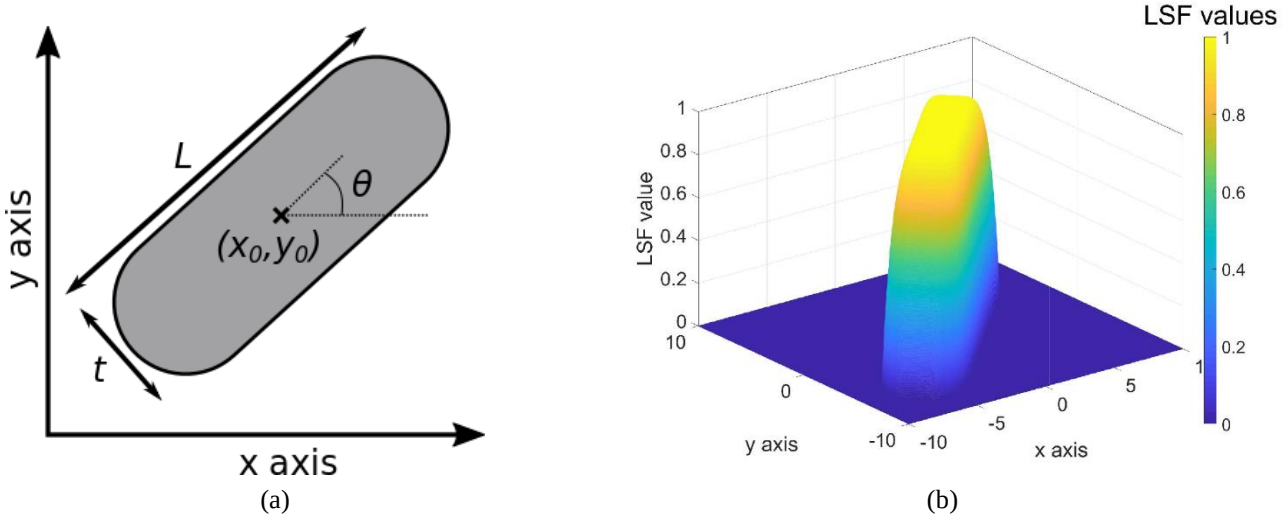

(a) (b)

Fig.2: MMC parameters (a) and corresponding LSF (b)

The choice of the criterion is important as it must balance exploration and accuracy in the area where the solution could be. A classic criterion is the Expected Improvement (EI) for the unconstraint problem, defined as [8]:

$$EI[\mathbf{p}] = \left(u_{peak}^{(best)} - \tilde{u}_{peak}(\mathbf{p})\right)\Phi\left(\frac{u_{peak}^{(best)} - \tilde{u}_{peak}(\mathbf{p})}{s(\mathbf{p})}\right) + s(\mathbf{p})\phi\left(\frac{u_{peak}^{(best)} - \tilde{u}_{peak}(\mathbf{p})}{s(\mathbf{p})}\right)$$

where $u_{peak}^{(best)}$ is the best solution found so far, $\tilde{u}_{peak}(\mathbf{p})$ the kriging meta-model prediction of the objective function at $\mathbf{p}$ at the current iteration, $s(\mathbf{p})$ is the predicted standard deviation at $\mathbf{p}$, $\Phi(.)$ is the normal distribution of the normal law and $\phi(.)$ is the normal law density function. The new point that should be added is the point that maximised the EI. For each configuration, the connectivity of the components is checked first. If it is unconnected the EI is set to a negative value to avoid these configurations.

In the case of a constraint optimisation problem, the EI is penalised to take into consideration the probability that the constraint will also be satisfied. The kriging surrogate model at $\mathbf{p}$ of the constraint is denoted $\tilde{g}$ and follows a normal law of parameters $(\tilde{\mu}, \tilde{s}^2)$. Yet $\frac{\tilde{g}-\tilde{\mu}}{\tilde{s}} \sim N(0,1)$, thus the feasibility probability, denoted $P(\mathbf{p})$, is [8]:

$$P(\tilde{g}(\mathbf{p}) \leq 0) = P\left(\frac{(\tilde{g}-\tilde{\mu})}{\tilde{s}} \leq -\frac{\tilde{\mu}}{\tilde{s}}\right) = \frac{1}{\sqrt{2\pi}}\int_{-\infty}^{-\tilde{\mu}/\tilde{s}} \exp\left(-\frac{\tilde{s}^2}{2}\right) ds$$

The Constrained Expected Improvement is then equal to:

$$CEI(\mathbf{p}) = EI[\mathbf{p}] * P(\mathbf{p})$$

The new point to be added to the learning set is the point that maximises this criterion. It is solved by using a genetic algorithm coupled with a gradient evaluation of the CEI [9]. In this case, the best point taken in the computation of the EI is the point that minimises the objective function and that satisfies the constraint.

Nonlinear analysis

Because of the contact nonlinearity, the vibration amplitude at resonance is obtained from a nonlinear analysis. The equation of motion of the system is:

$$\mathbf{M}\ddot{\mathbf{x}}(t) + \mathbf{C}\dot{\mathbf{x}}(t) + \mathbf{K}\mathbf{x}(t) + \mathbf{F_{nl}}\left(\mathbf{x}(t), \dot{\mathbf{x}}(t)\right) = \mathbf{F_e}(t)$$

With **M, C** and **K** the mass, damping and stiffness matrices respectively, **x** the vector of retained dof, $\mathbf{F_{nl}}$ the vector of nonlinear forces and $\mathbf{F_e}$ the vector of the excitation force. The mass and stiffness structural matrices are obtained from a Craig-Bampton reduction of the full system matrices. Retained dof corresponds to the contact nodes, excitation dof (for the platform), output node (for the platform) and a set of modes, so the size of the matrices will change as the number of contact nodes will change during the optimisation. The number of modes is kept constant for numerical reasons and high values used to ensure the accuracy of the reduced system for all cases (12 modes for the platform and 30 for the damper). A Rayleigh damping matrix of 0.2% is adopted for each component to ensure numerical convergence even when the friction damping is low. For the full damper case, the size of the problem is 454. Before the Craig-Bampton reduction, the LSF is projected onto the initial mesh of the damper. To avoid localised modes, void elements are removed.

The problem is solved with the well-established harmonic balance method (HBM) [10], where the periodic solution **x** is approximated by a truncated Fourier expansion of cosine coefficients $\mathbf{x}_k^{(C)}$ and sine coefficients $\mathbf{x}_k^{(S)}$ with N_h harmonics and grouped in the vector **q**. The EOM in the Fourier domain that must be solved is:

$$\mathbf{J_1}(\mathbf{q}, \omega) = \mathbf{Z}(\omega)\mathbf{q} + \tilde{\mathbf{F}}_{\mathbf{nl}}(\mathbf{q}) - \tilde{\mathbf{F}}_e = 0$$

To avoid the computation of the full frequency response function with a continuation algorithm, the resonance is directly obtained by adding a phase constraint to the previous equation [11], it translates the idea that at resonance the phase ϕ between the excitation and the output is equal to $\frac{\pi}{2}$:

$$J_2(\mathbf{q}, \omega) = \phi - \frac{\pi}{2} = 0$$

The angular frequency becomes an unknown of the problem and one must find $\boldsymbol{\alpha} = [\mathbf{q}, \omega]$ that satisfies $[\mathbf{J_1}(\mathbf{q}, \omega), J_2(\mathbf{q}, \omega)] = \mathbf{0}$. It is solved with a trust region dogleg algorithm.

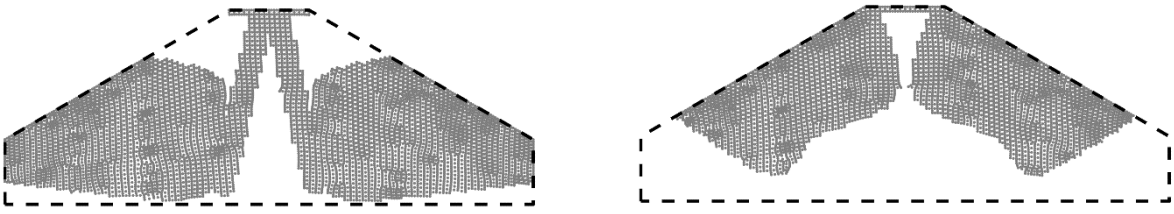

(a) (b)

Fig.3: Example of damper geometries that do not satisfy the stress constraint (elements with density inferior to 0.5 are removed for the sake of readability)

Static stress analysis

Previous works have raised a concern about optimised geometries that have extremely thin parts, and so not able to ensure the reliability of the damper in working conditions. For this reason, a constraint is added on the static stress distribution over the damper. The LSF must first be carefully projected on the initial mesh in order to avoid localised stress peak at the domain boundaries. For an element that is at the boundary, an intermediary density d_i is allocated defined as [3,4,5]:

$$\mu_i = \frac{1}{S_i} \times \int_{(x,y)\in elem_i} H\ o\ \Psi(x,y)dxdy$$

Where S_i is the surface of the element i, H the Heaviside function and Ψ the global LSF. Then, the Young modulus of the element is modified and equals $E_i = (1-\mu_i)E_{erstaz} + \mu_i E_0$, where E_0 is the Young modulus of the material and E_{ersatz} the Young modulus of the ersatz material (taken equal to $10^{-3}E_0$). For void elements, the Young modulus is set to the ersatz Young modulus. Similarly, the density is also updated.

The stress computation is done in Abaqus. The damper is subjected to different loadings, namely the centrifugal loading and the contact forces. The centrifugal loading of the element i is $C_F^{(i)} = m_i d_i \omega^2$, with m_i the mass of the element and d_i the distance to the rotation centre (taken as the distance to the centre of the base here). Contact forces are decomposed as a normal component N and a tangential one T. The von Mises stress constraint limit is taken equal to $\sigma_{\text{lim}} = 100MPa$. It has proved to be a good threshold to remove geometries with thin parts or with sharp angles. As an illustration, example of geometries that do not satisfy the stress constraint (and so that are removed) are given in Fig.3.

RESULTS

Optimisation parameters

In this work, five components are employed to describe the damper geometry. A few assumptions are made to take into consideration physical and engineering constraints, but also to reduce the number of optimisation parameters. First, one component is set to a horizontal position at the top of the damper with a small thickness (about one element thickness) to seal the platforms. Second, the damper is assumed to be symmetric about its central axis. Third, to ensure the existence of the contact between the damper and the platform, the centre of one component must be on the contact line (i.e. vertical and horizontal positions of one component are dependent). With these different choices, the optimisation problem is of size 9.

The objective is to minimise the objective function, which is the vibration amplitude at resonance obtained from the nonlinear analysis, under a static stress constraint. To improve the efficiency of the algorithm, the objective function is modified. Instead of optimising the vibration amplitude at resonance (denoted u_{peak}), the inverse of the opposite of the latter is optimised, i.e. $f_{peak} = -1/u_{peak}$. This is motivated by the idea that the vibration amplitudes are small and this transformation tends to spread the objective function values, and so it makes the optimisation more robust.

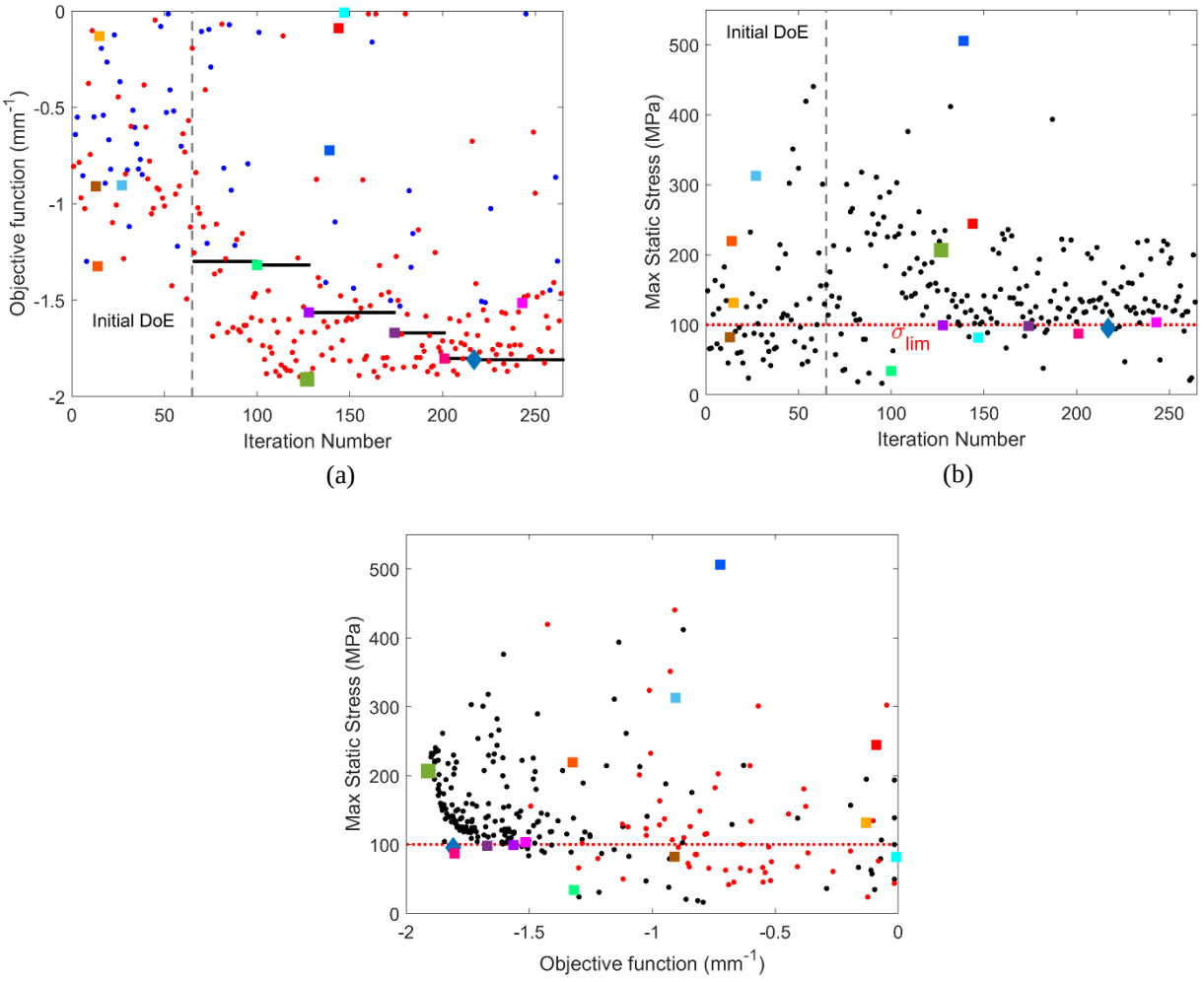

Fig.4: (a) Evolution of the objective function versus iteration number – (•) best current minimum - (•) configuration that satisfies the constraint limit - (•) configuration that doesn't satisfy the constraint limit
(b) Evolution of the constraint function versus iteration number – (- - -) constraint limit
(c) Pareto front between the objective function and the constraint function - (•) initial DoE
(♦) best configuration that satisfies the constraint
(■) best configuration without constraint consideration
(■) damper geometries represented in Figure 6

Optimisation results

As a first illustration of the results, the evolution of the objective function and of the constraint versus the iteration number as well as the objective function versus the maximum stress are given in Figure 4. In Figure 4a, blue points denote configurations for which the constraint is satisfied, and red points configuration for which the constraint is not satisfied. The black dots are the best current minimum that satisfy the constraint. The blue diamond is the best configuration that satisfies the constraint and the green square the best configuration without constraint consideration. In Figure 4c, red points denote points that are in the initial DoE, and black points configurations obtained during the optimisation part.

One can see that in the initial design, the objective function takes values between -1.5 mm^{-1} and 0 mm^{-1} and about half the geometries satisfy the constraint. As soon as the optimisation starts, the objective function takes value between -2 mm^{-1} and -1.5 mm^{-1} most of the time, which demonstrates the ability of the algorithm to identify quickly more efficient damper geometries. Optimal damper geometries that reduce the vibration amplitude at resonance but also verify the stress constraint are identified iteratively. At the end, the best geometry that satisfies the constraint gives a vibration amplitude at resonance of 0.55 mm and a maximal stress of 95.3 MPa. It is represented in Figure 5a. The damper geometry that has the highest damping properties gives a vibration amplitude of 0.52 mm, but has much higher level of stress (equal to 206.4 MPa). It is represented in Figure 5b. Considering the Figure 4c where the objective function versus the maximum stress are given, one can see that geometries associated with the lowest level of vibrations at resonance also have higher level of stress and a Pareto front is observable. Without stress consideration, the optimal

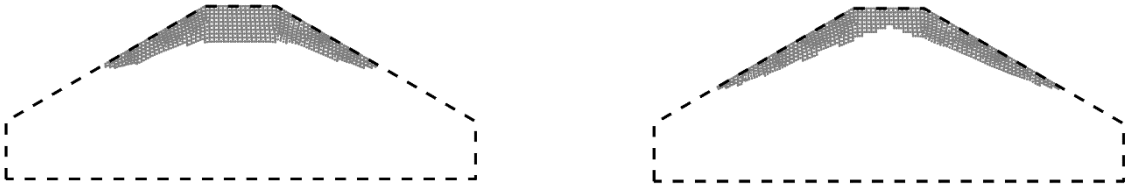

(a) (b)

Fig.5: (a) Best geometry that satisfies the stress constraint and (b) best geometry that doesn't satisfy the stress constraint – Dashed lines represent the limit of the full damper – Material domain in grey (elements with a low density are removed for the sake of readability)

geometry tends to have a shape composed of two thin arms. With this shape, the damper mass is reduced and the contact surface is increased which tends to maximise the number of contact points experiencing stick-slip. However, it also gives higher level of stress in the damper. By adding a stress constraint, the material is more located on the top of the damper. The global shape can be considered as similar (two thin arms), but with thicker arms that gives a better stress distribution in the damper.

Different damper geometries are represented in Figure 6. Each geometry is identified with a coloured square that refers to results given in Figure 4. Geometries of the first line are geometries from the initial DoE. One can see they have various and unusual shapes. Some of them have thin parts (see the yellow one for example) or thin junctions between the left and right parts on the damper that are at the origin of stress concentration (see the orange one). Geometries on the second lines are the different geometries that correspond to the best current minimum satisfying the constraint function. If strong variations in terms of shape are observed at the beginning, the algorithm converges quickly to the final geometry as the two last geometries are very close to the final one. Finally, geometries on the last line are displayed to illustrate the large variety of geometries that are tested during the optimisation and how the compromise between damping properties and stress constraint might be difficult to meet. Indeed, the light blue and red geometries verify the stress constraint but have low damping efficiency. The blue one has low damping efficiency and presents high level of stress. Finally, the pink one is located near the constraint limit and so has satisfactory damping properties and acceptable stress levels. It demonstrates that the approach is able to go all over the design space, but is also able to optimise finely the final geometry.

To compare with the full damper geometry, the principal characteristics are summarized in the Table 1. Both optimal geometries represent a drastic reduction of the damper mass (about 90% mass reduction compared to the full damper). The optimal geometry that satisfies the stress constraint presents a frequency shift of about 25 Hz at resonance compared to the full damper case, and a shift of 29 Hz is observed for the other geometry. In terms of damping, both geometries present a substantial reduction of the vibration amplitude at resonance for the blade as it is reduced by 67% and 68%, respectively. So, both geometries have similar dynamic properties, and finally their main difference relies in the static stress.

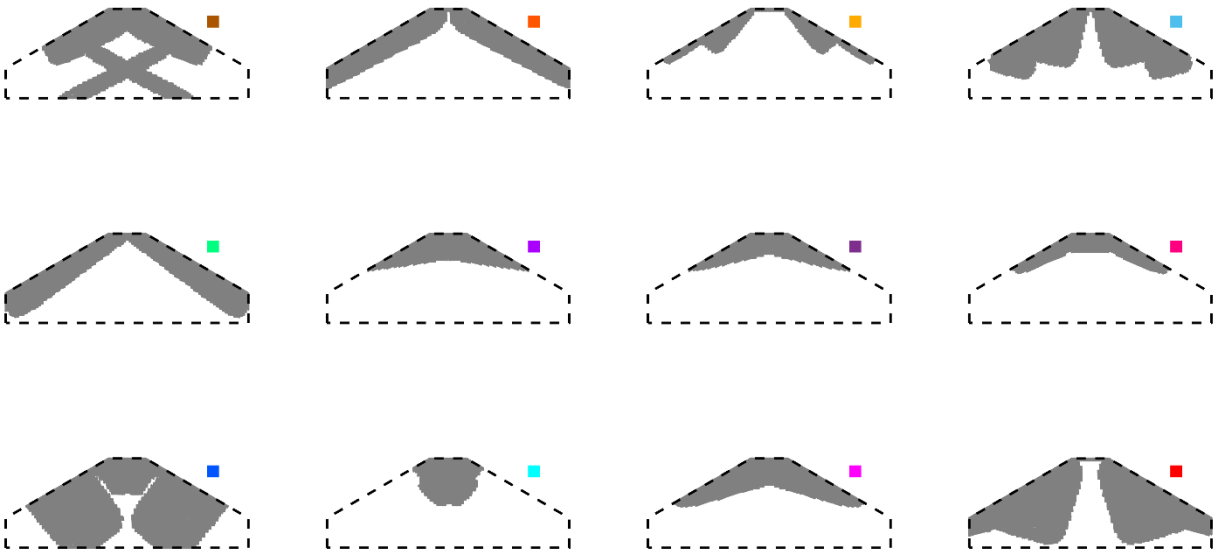

Fig.6: Different damper geometries tested during the optimisation

As the dynamic properties are strongly related to the contact point status (stick-slip, impact or separation), the contact information is summarized in the Table 2. Between the two geometries, the contact surface varies a lot (70 contact points for one case, and 52 contact point for the other case) and so the initial contact normal loading is strongly impacted (see variations of N0). However, the ratio of contact points in stick-slip remains the same and is about 75%. Despite the difference in terms of geometry, the ratio of contact points that dissipate energy is similar, which explains the good damping properties of the optimal geometry despite its smaller contact surface and higher contact normal load (which delays the entering of stick-slip for contact points). In comparison, for the full damper, the number of points in stick-slip condition represents only 5% of the number of contact points, which explains the lower damping properties of the latter.

	Mass ratio	**Resonance freq. (Hz)**	**Amplitude at resonance (mm)**	**Max. stress (MPa)**
Full damper	1	403.57	1.63	51.42
Best with constraint	0.1095	378.71	0.55	95.3
Best without constraint	0.1090	374.74	0.52	206.4

Tab.1: General characteristics of the different damper geometries

	N0 (N)	**Nb contact points**	**Nb points in stick-slip**	**Nb points in impact**	**Nb points in stuck**
Full damper	9.8987	102	5	1	96
Best with constraint	2.2292	52	38	14	0
Best without constraint	1.6428	70	52	18	0

Tab.2: Contact characteristics of the different damper geometries

CONCLUSION AND PERSPECTIVES

Constrained topological optimisation for nonlinear vibrations due to contact friction has been presented here. The general approach is based on the MMC framework and the EGO algorithm for the optimisation. Kriging surrogate models of the objective function and of the constraint function are constructed. The shape of an underplatform damper has been optimised to minimise the vibration amplitude at resonance with the consideration of a constraint on the static stress. By adding this constraint, non-reliable geometries with thin parts are eliminated during the optimisation. The final optimal geometry that satisfies the stress constraint has a mass distribution over the design space that is more localised on the top of the damper compared to the geometry that just minimises the nonlinear resonance. However, despite their shape difference and the difference in the contact surface, both geometries have a ratio of contact points in stick-slip that is equal and have no points in stuck condition. Future works will be dedicated to the extension to 3D and experimental validation.

Acknowledgements
E. Denimal and L. Salles have received funding from Rolls-Royce and the EPSRC under the Prosperity Partnership Grant CornerStone (EP/R004951/1). L. Renson has received funding from the Royal Academy of Engineering (RF1516/15/11). E. Denimal has received funding from Rennes Metropole. Rolls-Royce, the EPSRC, the Royal Academy of Engineering and Rennes Metropole are gratefully acknowledged.

REFERENCES

[1] Krack, M., Salles, L., & Thouverez, F. (2017). Vibration prediction of bladed disks coupled by friction joints. *Archives of Computational Methods in Engineering*, *24*(3), 589-636.

[2] Denimal, E., Wong, C., Salles, L., & Pesaresi, L. (2021). On the Efficiency of a Conical Underplatform Damper for Turbines. *Journal of Engineering for Gas Turbines and Power*, *143*(2), 021020.

[3] Sigmund, O., & Maute, K. (2013). Topology optimization approaches. *Structural and Multidisciplinary Optimization*, *48*(6), 1031-1055.

[4] Guo, X., Zhang, W., & Zhong, W. (2014). Doing topology optimization explicitly and geometrically—a new moving morphable components based framework. *Journal of Applied Mechanics*, *81*(8).

[5] Raponi, E., Bujny, M., Olhofer, M., Aulig, N., Boria, S., & Duddeck, F. (2019). Kriging-assisted topology optimization of crash structures. *Computer Methods in Applied Mechanics and Engineering*, *348*, 730-752.

[6] Denimal, E., El Haddad, F., Wong, C., & Salles, L. (2021). Topological Optimization of Under-Platform Dampers With Moving Morphable Components and Global Optimization Algorithm for Nonlinear Frequency Response. *Journal of Engineering for Gas Turbines and Power*, *143*(2), 021021.

[7] Denimal, E., Renson, L., & Salles, L. (2021). Topological optimisation of friction dampers for nonlinear resonances mitigation. In *Nodycon 2021*.

[8] Pesaresi, L., Salles, L., Jones, A., Green, J. S., & Schwingshackl, C. W. (2017). Modelling the nonlinear behaviour of an underplatform damper test rig for turbine applications. *Mechanical Systems and Signal Processing*, *85*, 662-679.

[7] Petrov, E. P., & Ewins, D. J. (2006). Advanced modelling of underplatform friction dampers for analysis of bladed disc vibration. In *Turbo Expo: Power for Land, Sea, and Air* (Vol. 42401, pp. 769-778).

[8] Jones, D. R., Schonlau, M., & Welch, W. J. (1998). Efficient global optimization of expensive black-box functions. *Journal of Global optimization*, *13*(4), 455-492.

[9] Mebane Jr, W. R., & Sekhon, J. S. (2011). Genetic optimization using derivatives: the rgenoud package for R. *Journal of Statistical Software*, *42*(1), 1-26.

[10] Detroux, T., Renson, L., Masset, L., & Kerschen, G. (2015). The harmonic balance method for bifurcation analysis of large-scale nonlinear mechanical systems. *Computer Methods in Applied Mechanics and Engineering*, *296*, 18-38.

[11] Renson, L., Hill, T. L., Ehrhardt, D. A., Barton, D. A. W., & Neild, S. A. (2018). Force appropriation of nonlinear structures. *Proceedings of the Royal Society A: Mathematical, Physical and Engineering Sciences*, *474*(2214), 20170880.